Evolutionary Optimization of Optical Antennas

Thorsten Feichtner, Oleg Selig, Markus Kiunke, and Bert Hecht

Nano-Optics & Biophotonics Group, Department of Experimental Physics 5, Röntgen Research Center for Complex Materials (RCCM), Physics Institute, University of Würzburg, Am Hubland, D-97074 Würzburg, Germany

(Received 24 April 2012; published 19 September 2012)

The design of nanoantennas has so far been mainly inspired by radio-frequency technology. However, the material properties and experimental settings need to be reconsidered at optical frequencies, which would entail the need for alternative optimal antenna designs. Here we subject a checkerboard-type, initially random array of gold cubes to evolutionary optimization. To illustrate the power of the approach, we demonstrate that by optimizing the near-field intensity enhancement, the evolutionary algorithm finds a new antenna geometry, essentially a split-ring–two-wire antenna hybrid that surpasses by far the performance of a conventional gap antenna by shifting the $n = 1$ split-ring resonance into the optical regime.

DOI: 10.1103/PhysRevLett.109.127701 PACS numbers: 84.40.Ba, 02.60.−x, 73.20.Mf, 78.67.Bf

Light-matter interaction, i.e., the absorption and emission of light as well as the control of its spectral and directional properties, can be optimized by means of antennalike plasmonic nanostructures [1,2]. This is of immediate importance in diverse fields of research, ranging from solar energy conversion [3], photocatalytic [4], and sensing applications [5] to single-particle manipulation [6,7] and spectroscopy [8], as well as quantum optics and communication [9–12].

The designs of rf antennas are usually optimized for the utilization of thin, infinitely good conducting wires that support surface currents and are typically fed by transmission lines with infinitely narrow gaps [13]. For antennas at optical frequencies, the general operation conditions deviate substantially from such ideal behavior. (i) Antenna wire diameters are comparable to the electromagnetic penetration depth into the wire material leading to volume currents [14]. In the case of noble metals, such wires therefore exhibit plasmon resonances in the visible spectral range, resulting in the reduced effective wavelength of wire waves [15]. (ii) The feeding (excitation) of optical antennas is often achieved with focused laser beams or quantum emitters. (iii) High-frequency-related effects such as ''kinetic inductance'' become significant [16]. It cannot therefore be taken for granted that rf-inspired antenna designs, such as dipole [17], bow-tie [18,19], and Yagi-Uda antennas [20,21], represent the ''optimal'' geometries also at optical frequencies—although they provide a reasonable performance.

Evolutionary algorithms (EAs) find the optimized solutions to highly complex nonanalytic problems by creating subsequent generations of individuals who are coded by their respective genomes that compete for the right to pass on their properties in accordance with a fitness parameter [22]. These optimized solutions can then be analyzed to foster the understanding of underlying physical principles. Evolutionary optimization has been applied successfully in various fields of research, including pulse shape optimization in the coherent control of chemical reactions [23] and field localization in plasmonic structures [24,25]. Furthermore, evolutionary optimization has been used to aid the development of radio-wave antennas [26,27]. Initial attempts to employ such methods to find improved plasmonic nanostructures have also been undertaken [28–31]; however, the investigated configurational space remained very limited.

Here, we employ the evolutionary optimization method in a more general setup to find improved plasmonic antenna structures that, in terms of near-field intensity enhancement (fitness parameter), outperform the best radio wave—type reference antennas by a factor of 2. Analyses of the fittest antenna reveal that it is a split-ring—two-wire antenna hybrid (split-ring antenna [SRA]), which merges the features of the fundamental magnetic resonance of a split-ring with the fundamental electric resonance of a linear dipole antenna—both in the visible wavelength regime.

Methods.—As fitness parameter, we choose the normalized near-field intensity enhancement in the focus of an illuminating Gaussian beam ($\lambda_i = 647$ nm, $NA = 1$, 4.3 fs pulse duration, 144 nm bandwidth). A genetic representation of complexly shaped thin-film nanoantennas is realized by composing structures (matrix antennas) from discrete gold cubes having fixed dimensions ($10 \times 10 \times 11$ nm^3), positioned on a 21×21 square matrix in vacuum, oriented perpendicular to and centered on the optical axis of the Gaussian beam. The fields of such structures can be described by local Maxwell equations.

The resulting configuration space of about 4×10^{132} different individual structures ensures geometrical variety but is impossible to explore by brute force methods, since the evaluation of an individual structure takes about 20 min. The size of the focal spot and the area occupied by the gold cube matrix are comparable (see Fig. S1 in

Supplemental Material [32]). An example showing a bow-tie antenna represented in a 5×5 array is depicted in Fig. 1. The genetic information is represented in a unique binary code, where the matrix elements are set to "1" if occupied by a gold cube and "0" when empty (for a calculation of the number of physical redundant structures, see Figs. S2 and S3 and the related discussion in Supplemental Material [32]).

We solve Maxwell's equations using the finite-difference time-domain (FDTD) method [33] (FDTD Solution, Lumerical Inc., Canada). Due to the discretization in space (Yee Cells, $dx = 1$ nm), adjacent gold cubes are fully connected to each other. We also obtain conductive bridges between the neighboring gold blocks that contact each other via their edges. All simulation objects were shifted by half a Yee cell size in the x and y direction to ensure identical dimensions of gold cubes and voids. In order to describe the dielectric function of gold in a sufficiently wide spectral range, we use the data by Johnson and Christy fitted by an analytical model [34,35].

The EA is implemented in MatLab [36]. It uses generations consisting of 20 or 30 individual matrix antennas. The five best structures based on the fitness parameter are selected as parents for the next generation. With carefully chosen mechanisms for crossover and mutation of the genomes, consecutive generations constantly improve in the sense that their fitness parameter increases. New descendants are created by first selecting one of the five parents by the roulette-wheel selection method [22] with a probability proportional to its fitness. Three methods, i.e., the creation of random structures, mutation, as well as linear and spiral genome crossing, are then applied, until a total of 20 (or 30) new individuals are generated for the next generation (see Fig. S4 in Supplemental Material [32]).

After a sufficient amount of generations have been simulated, a so-called toggle plot analysis is performed, which consists of running 21×21 simulations in which every block is toggled individually. Color coding the block positions according to the magnitude of the fitness changes

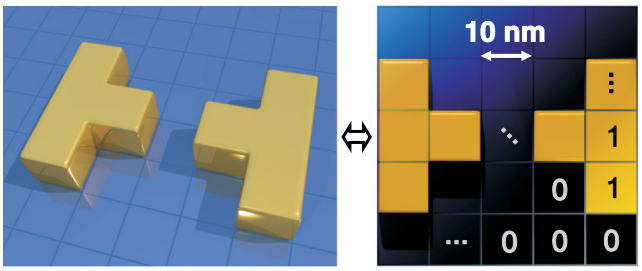

FIG. 1 (color online). Genetic representation of a matrix antenna. Left: artistic three-dimensional view of an example bow-tie nanoantenna consisting of eight gold cubes. Right: top view indicating the transition to a 5×5 matrix representation, where each "1" denotes the presence of a $10 \times 10 \times 11$ nm^3 block of gold.

associated with the individual toggle event shows the relative importance of single blocks and the potential for further improvement of the matrix antenna, and also eventually produces new individuals with enhanced fitness [37].

Results.—The wavelength λ_i coincides with the resonance of a linear dipole nanoantenna consisting of two end-to-end aligned $46 \times 30 \times 11$ nm^3 gold rods (width = 3 cubes, height = 1 cube) separated by a 10 nm gap [Fig. 2(a), top panel], which serves as a reference structure. This exhibits a resonant normalized near-field intensity enhancement of about 1800 in the center of its feed gap. Other geometries, such as bow-tie antennas, do not yield higher fitness.

In the following, we discuss the fittest structure obtained by running the EA for 100 generations with 20 individuals each (see Fig. S5 in Supplemental Material [32] for development of the geometry and fitness parameter), a subsequent toggle plot analysis, and further 30 generations with 30 individuals each, starting with combinations of the best five structures obtained from the toggle plot analysis.

The best matrix antenna structure [Fig. 2(a), lower panel] exhibits a remarkably high fitness, as indicated by its near-field spectrum in Fig. 2(b), which is recorded in the optimization point [indicated as blue dot in Fig. 2(a)] after a broadband excitation. Its maximal near-field intensity enhancement of 3500 is nearly twice as high as that of the reference antenna. Both spectra show single, nearly Lorentzian peaks ($Q = 20$ and 23; see Supplemental Material [32] for a further discussion of the Q-factor).

According to the reciprocity theorem [1,2], the optimized antenna should also improve the radiative properties of a quantum emitter positioned in the spot of highest field enhancement. Indeed, for the reference antenna we find a radiation enhancement of 2126 and a radiation efficiency of 0.255, while for the fittest antenna the radiation enhancement is 4271, with radiation efficiency of 0.268. Surprisingly, the directivity of the fittest antenna remains very similar to that of the reference antenna, despite its complex shape (see Fig. S6 and related discussion in Supplemental Material [32]).

The fittest matrix antenna exhibits three noticeable geometrical features: (i) a small gap in the center between two compact rod(like) structures, slightly displaced in the y direction with respect to the observation point. (ii) a single gold block directly below the gap, which creates a current path connecting the rod-like structures, and (iii) a seemingly random arrangement of gold blocks further away from the center. It is important to note that the optimal structure found by a genetic algorithm depends on both the available primitive elements as well as the possible boundary conditions.

We now consider the near-field intensity enhancement maps of both the reference and matrix antennas in Fig. 2(c). The small displacement of the rodlike structures increases the near-field intensity enhancement by a small factor

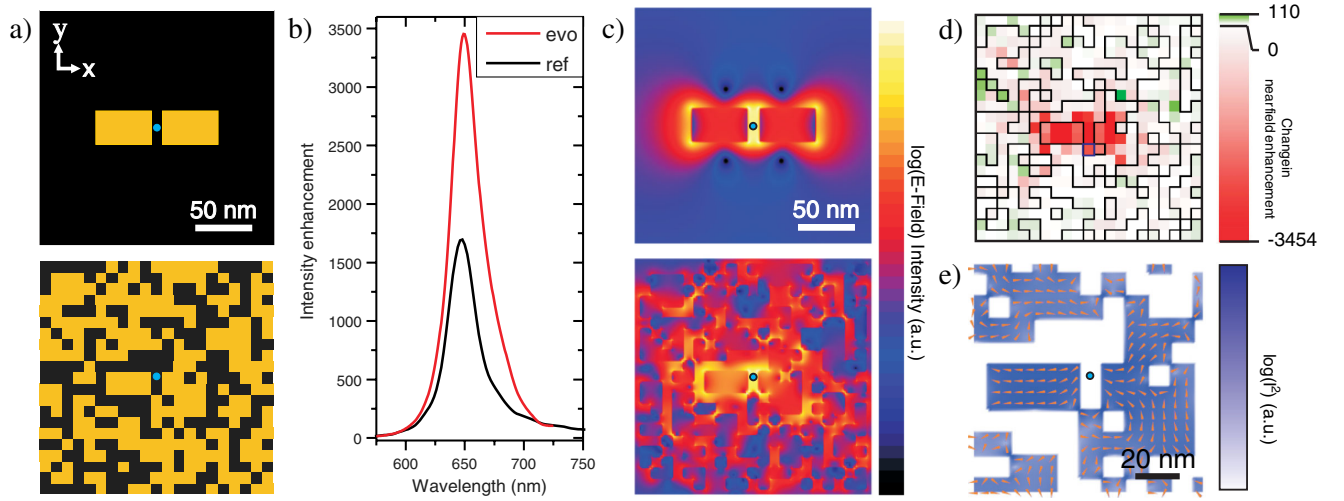

FIG. 2 (color online). Comparison at $\lambda = 647$ nm between a resonant linear dipole nanoantenna built from two 10-nm separated rectangular arms of $46 \times 30 \times 11$ nm^3 and a structure obtained with the EA described in the text. (a) shows the geometry of both structures from the $+z$ direction. The blue spot denotes the position of the near-field optimization by the EA. The spectra in (b) are taken at this marked position during a broadband Gaussian excitation. (c) shows the logarithmic near-field intensities at $\lambda = 647$ nm when the structures are illuminated by a monochromatic Gaussian focus with $NA = 1$. The scales are normalized and not comparable. In (d) the the change of near-field enhancement at the optimization position is shown for each single block when it is toggled. (e) is a zoom of the central part of the EA antenna, showing the strength and direction of the currents.

because of the proximity of the corners of the rodlike structures to the point of optimization. However, this alone cannot by far explain the observed increase of the near-field intensity enhancement. The achievable enhancement by displacing the reference antenna in a similar way amounts to a factor of 1.1.

The results of a toggle plot analysis are shown in Fig. 2(d). The results indicate that the toggling of individual blocks does not result in considerable additional near-field intensity enhancement, but rather causes a severe reduction. We therefore believe that the structure's fitness is close to a (local) maximum in the configuration space. By far the strongest reduction of fitness occurs when toggling gold blocks near the center. This indicates that the compact structure in the proximity of the gap dominates the field enhancement and is most critical for achieving the observed performance. Assuming that it is excited at an eigenmode, this also explains the appearance of a single narrow Lorentzian resonance. As apparent from the toggle plot, the random structures far away from the center do hardly influence the field enhancement in the gap. Nevertheless, it is possible that the collective effects of the peripheral blocks do influence the fitness of the structure to some extent; however, due to the inherent complexity involved, we will not be discussing this further in detail.

Of particular interest is the single gold block below the gap. This provides a current path via the cube edges between the two rodlike structures that form the gap, as can be seen by taking a closer look at the currents in the central part of the matrix antenna in Fig. 2(e). Surprisingly, we find that removing this block greatly lowers the fitness of the resulting matrix antenna, instead of increasing it. A closer inspection of Fig. 2(e) reveals two particular current paths, one located in the rodlike structures, corresponding to a bonding linear dipolar nanoantenna mode, and the other, flowing from one upper gap edge through the connecting gold block to the other upper gap edge, corresponding to a fundamental split-ring mode.

In order to better understand the effects that lead to the increased near-field intensity enhancement, in the following we study a reduced model system, i.e., a mixture of a split-ring and a linear two-wire antenna, called the split-ring antenna, which retains the important features of the fittest matrix antenna but can be described by a small number of freely tunable parameters. Its geometry is depicted in Fig. 3(a). The structure can be interpreted either as a linear two-wire antenna with an asymmetric short circuit, a split-ring resonator with attached wires, or a long single nanowire that is deformed in a particular way.

The near-field intensity enhancement of the SRA in the center plane is depicted in Fig. 3(b), showing a strong field concentration toward the open side of the SRA gap, as already observed in the best matrix antenna. Figure 3(c) compares the spectra of the resonances of a SRA with a nonshort-circuited dipolar antenna of identical arm cross section, gap size, and resonance frequency. Both spectra were obtained at the point of highest near-field enhancement along the y axis. Also, in the reduced model system, the split-ring antenna surpasses the classical dipole antenna design in terms of maximum near-field intensity enhancement by a factor of 2.

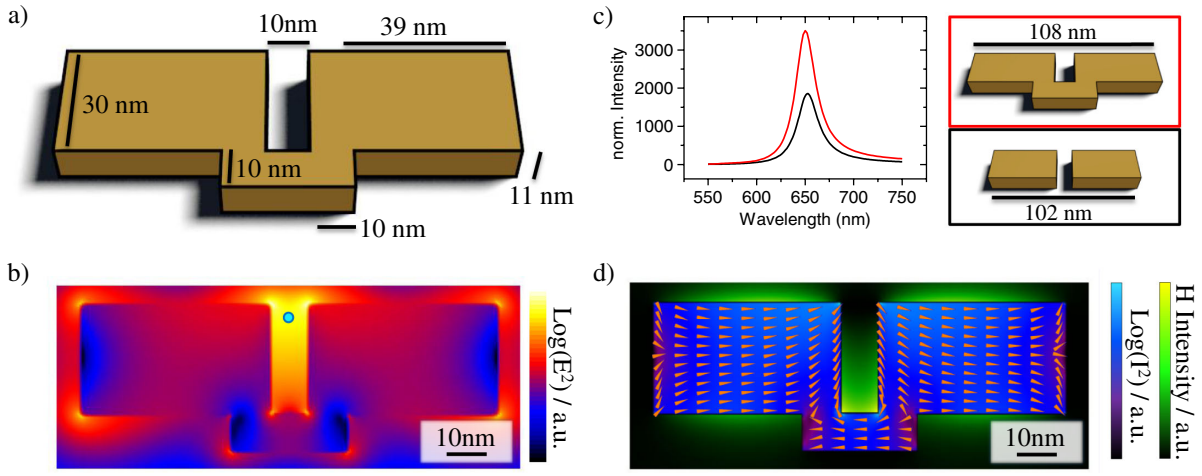

FIG. 3 (color online). (a) Geometry and dimensions of the examined split-ring antenna. (b) Near-field intensity enhancement of the structure in (a), showing highly concentrated fields towards the open end of the gap. The blue point denotes the point of the measurement for the spectrum figured in (c). The $Q \approx 25$ for the SRA grey (red online) is comparable to that of the reference antenna (black). (d) shows an overlay of the squared current density and the current direction inside the material as well as the magnetic near-fields outside the structure.

The current pattern in the reduced model system can be decomposed into a fundamental ($n = 1$) split-ring mode [38] and a dipolar current in each antenna arm running 180° out of phase to the current in the short circuit [Fig. 3(d)], adding to the charge accumulation in the upper part of the gap and thus increasing the near-field intensity enhancement. Since the resonance is in the optical regime, the SRA is one way to circumvent the limitation of pure split-ring resonances to wavelengths above 900 nm due to kinetic inductance [16]. The SRA represents a magnetic dipole in the visible range, showing magnetic fields [Fig. 3(d)] that are only by factor of 2.5 weaker than those of the isolated split-ring resonator at a resonance wavelength of 908 nm.

To confirm the shift of the fundamental split-ring mode from the infrared into the visible spectral range, we place two gold bars ($35 \times 30 \times 11$ nm^3) separated by a 5 nm nonconductive gap from the isolated split-rings ends. The extinction cross section is examined while connecting the gold bars with the split-ring via successively thicker gold bridges at the center of the gap (see Fig. 4 and the inset). In the unconnected geometry, the fundamental split-ring resonance is shifted into the red to about 1200 nm due to capacitive coupling across the gap. As the connection grows thicker (increasing d), the fundamental split-ring mode is shifted by more than 500 nm from the infrared into the visible range. The shift of the resonance is of similar origin as the emergence of a charge transfer mode for a dipolar antenna due to a conductive bridge [39]. However, here the fundamental split-ring mode does not disappear, but its phase is inverted (compare the charge distributions sketched in the lower panel of Fig. 4). For very thin conductive bridges, both modes coexist (see also Ref. [39]) and cancel out each other, leading to a dip in the extinction cross section.

Conclusion.—We show that by using the method of evolutionary optimization in a large parameter space, high-fitness plasmonic antennas can be found within a reasonable amount of time. The method can be adapted to a large variety of fitness parameters in order to optimize plasmonic structures for various purposes. Besides directly yielding optimized structures, a careful analysis of the working principles of the resulting geometries may provide new design strategies for high-performance plasmonic nanostructures.

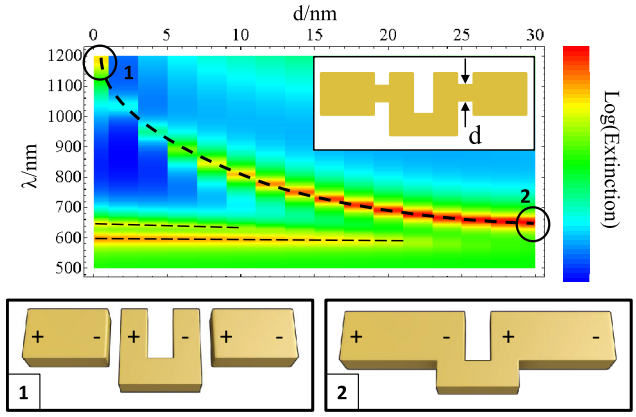

FIG. 4 (color online). Wavelength shift of the extinction cross section resonance for the combined two-wire antenna and the $n = 1$ split-ring resonance, as the conductive link between the two antenna rods and the split-ring (see inset) increases in thickness (marked thick dashed). Also visible are the bonding and antibonding $n = 3$ modes, which also shift slightly into the blue and get very weak (marked thin dashed). The sketches at the bottom show the geometries of the fully disconnected and fully connected structures, together with the position and sign of their mode's charge density maxima.

In the present example, we obtain an increase of the near-field intensity enhancement by nearly a factor of 2, caused by the intriguing cooperation of a fundamental split-ring mode and dipole antenna resonance. We have used the latter principle to devise a novel antenna design that additionally exhibits very large magnetic fields at optical frequencies. In particular, the fundamental split-ring resonance is shifted into the visible spectral range because of the formation of a charge-transfer-like hybrid resonance with two rods of a dipolar antenna. The method can be further adapted to include geometrical constraints imposed by microfabrication and therefore lead to structures that can directly be implemented in practical applications.

The authors acknowledge P. Biagioni, C. Brüning, and J. C. Prangsma for fruitful discussions. Financial support by the DFG is gratefully acknowledged (HE5618/1-1).

[1] P. Bharadwaj, B. Deutsch, and L. Novotny, Adv. Opt. Photon. **1**, 438 (2009).
[2] P. Biagioni, J.-S. Huang, and B. Hecht, Rep. Prog. Phys. **75**, 024402 (2012).
[3] H. A. Atwater and A. Polman, Nature Mater. **9**, 205 (2010).
[4] Z. Liu, W. Hou, P. Pavaskar, M. Aykol, and S. B. Cronin, Nano Lett. **11**, 1111 (2011).
[5] J. Becker, A. Trügler, A. Jakab, U. Hohenester, and C. Sönnichsen, Plasmonics **5**, 161 (2010).
[6] M. L. Juan, R. Gordon, Y. Pang, F. Eftekhari, and R. Quidant, Nature Phys. **5**, 915 (2009).
[7] W. Zhang, L. Huang, C. Santschi, and O. J. F. Martin, Nano Lett. **10**, 1006 (2010).
[8] A. Kinkhabwala, Z. Yu, S. Fan, Y. Avlasevich, K. Muellen, and W. E. Moerner, Nature Photon. **3**, 654 (2009).
[9] A. V. Akimov, A. Mukherjee, C. L. Yu, D. E. Chang, A. S. Zibrov, P. R. Hemmer, H. Park, and M. D. Lukin, Nature (London) **450**, 402 (2007).
[10] R. Kolesov, B. Grotz, G. Balasubramanian, R. J. Stohr, A. A. L. Nicolet, P. R. Hemmer, F. Jelezko, and J. Wrachtrup, Nature Phys. **5**, 470 (2009).
[11] J.-S. Huang, T. Feichtner, P. Biagioni, and B. Hecht, Nano Lett. **9**, 1897 (2009).
[12] Z. Jacob and V. M. Shalaev, Science **334**, 463 (2011).
[13] C. A. Balanis, Proc. IEEE **80**, 7 (1992).
[14] J. Dorfmueller, R. Vogelgesang, W. Khunsin, C. Rockstuhl, C. Etrich, and K. Kern, Nano Lett. **10**, 3596 (2010).
[15] L. Novotny, Phys. Rev. Lett. **98**, 266802 (2007).
[16] J. Zhou, T. Koschny, M. Kafesaki, E. N. Economou, J. B. Pendry, and C. M. Soukoulis, Phys. Rev. Lett. **95**, 223902 (2005).
[17] P. Mühlschlegel, H.-J. Eisler, O. J. F. Martin, B. Hecht, and D. W. Pohl, Science **308**, 1607 (2005).
[18] P. J. Schuck, D. P. Fromm, A. Sundaramurthy, G. S. Kino, and W. E. Moerner, Phys. Rev. Lett. **94**, 017402 (2005).
[19] J. N. Farahani, D. W. Pohl, H.-J. Eisler, and B. Hecht, Phys. Rev. Lett. **95**, 017402 (2005).
[20] T. H. Taminiau, F. D. Stefani, and N. F. Van Hulst, Opt. Express **16**, 10858 (2008).
[21] A. G. Curto, G. Volpe, T. H. Taminiau, M. P. Kreuzer, R. Quidant, and N. F. van Hulst, Science **329**, 930 (2010).
[22] S. Sivanandram and S. Deepa, *Introduction into Genetic Algorithms* (Springer-Verlag, Berlin, 2008).
[23] T. Baumert, T. Brixner, V. Seyfried, M. Strehle, and G. Gerber, Appl. Phys. B **65**, 779 (1997).
[24] M. Aeschlimann, M. Bauer, D. Bayer, T. Brixner, F. J. García de Abajo, W. Pfeiffer, M. Rohmer, C. Spindler, and F. Steeb, Nature (London) **446**, 301 (2007).
[25] M. Aeschlimann, M. Bauer, D. Bayer, T. Brixner, S. Cunovic, F. Dimler, A. Fischer, W. Pfeiffer, M. Rohmer, C. Schneider, F. Steeb, C. Strüber, and D. V. Voronine, Proc. Natl. Acad. Sci. U.S.A. **107**, 5329 (2010).
[26] H. Huang, A. Hoorfar, and S. Lakhani, *Antennas and Propogation Society International Symposium, Honolulu, HI, 2007* (IEEE, New York, 2007), p. 1609.
[27] M. F. Pantoja, A. R. Bretones, S. Member, R. G. Martin, and S. Member, IEEE Trans. Antennas Propag. **55**, 1111 (2007).
[28] P. Ginzburg, N. Berkovitch, A. Nevet, I. Shor, and M. Orenstein, Nano Lett. **11**, 2329 (2011).
[29] S. Kessentini, D. Barchiesi, T. Grosges, and M. de la Chapelle, *Evolutionary Computation (CEC), 2011* (IEEE, New York, 2011), p. 2315.
[30] C. Forestiere, M. Donelli, G. F. Walsh, E. Zeni, G. Miano, and L. D. Negro, Opt. Lett. **35**, 133 (2010).
[31] C. Forestiere, A. J. Pasquale, A. Capretti, G. Miano, A. Tamburrino, S. Y. Lee, B. M. Reinhard, and L. Dal Negro, Nano Lett. **12**, 2037 (2012).
[32] See Supplemental Material at http://link.aps.org/supplemental/10.1103/PhysRevLett.109.127701 for additional information about the evolutionary algorithm and the fittest antenna structure.
[33] A. Taflove and S. C. Hagness, in *Computational Electrodynamics: The Finite-Difference Time-Domain Method*, edited by A. Taflove (Artech House, Inc., Boston, 2005), 3rd. ed.
[34] P. B. Johnson and R. W. Christy, Phys. Rev. B **6**, 4370 (1972).
[35] P. G. Etchegoin, E. C. L. Ru, and M. Meyer, J. Chem. Phys. **125**, 164705 (2006).
[36] All necessary codes written in the Lumerical script language or MatLab can be made available upon request.
[37] This is the brute force realization of the hill climber algorithm on our setup, neglecting pair- and higher-order correlations.
[38] C. Rockstuhl, F. Lederer, C. Etrich, T. Zentgraf, J. Kuhl, and H. Giessen, Opt. Express **14**, 8827 (2006).
[39] M. Schnell, A. Garcia-Etxarri, A. J. Huber, K. Crozier, J. Aizpurua, and R. Hillenbrand, Nature Photon. **3**, 287 (2009).